Scientia Iranica B (2014) 21(6), 1880–1895

Sharif University of Technology
Scientia Iranica
Transactions B: Mechanical Engineering
www.scientiairanica.com

A force reduced-order approach for optimal control of turbulent flow over backward-facing step using POD analysis and perturbation method

A. Zare[a,*], H. Emdad[b] and E. Goshtasbi Rad[b]

a. *Department of Mechanical Engineering, Marvdasht Branch, Islamic Azad University, Marvdasht, Iran.*
b. *School of Mechanical Engineering, Shiraz University, Shiraz, Iran.*

Received 18 September 2012; received in revised form 5 April 2014; accepted 29 April 2014

KEYWORDS
POD;
Galerkin projection;
Flow control;
Backward-facing step;
Perturbation;
RNG $k-\varepsilon$ model.

Abstract. In this article, a forced reduced-order modeling approach, suitable for active optimal control of fluid dynamical systems, based on the Proper Orthogonal Decomposition and perturbation method on the Reynolds-Averaged Navier-Stokes equations, is presented. Numerical simulation of turbulent flow equations is too costly for the purpose of optimization and control of unsteady flows. As a result, the POD/Galerkin projection and perturbation method on the RANS equations is considered. Using the perturbation method, the controlling parameter shows up explicitly in the forced reduced-order system. The feedback control of the controlling parameter is one of the objectives of this study. With the perturbation method, the effect of the controller is sensed by the fluid flow at each time step. The effectiveness of this method has been shown on optimal control of the re-circulation problem for a turbulent flow over a step with blowing/suction controlling jets. Actuators are positioned at two different locations; blowing/suction jets at the foot and edge of the step, and blowing/suction jets at the wall of the step. Results show that the perturbation method is fast and accurate in estimating the re-circulated turbulent flow over a step. It is concluded that blowing/suction jets at the wall of the step are more efficient in mitigating flow separation.

1. Introduction

Flow separation over a backward-facing step in a channel has a very simple geometry and, in the field of flow control, is gaining considerable attention. Various studies have been performed on controlling the location of the reattachment point behind backward-facing steps with both laminar and turbulent flow. These studies include passive and active control mechanisms. Passive control mechanisms incorporate fixed attachments to reduce or remove the separation bubble behind the backward facing step for a given range of operating conditions. Work on passive control mechanisms include the use of a permeable reattachment surface [1], various step heights [2], porous surfaces [3] and a row of three-dimensional surface humps [4]. The active control method is performed using a different mechanism. Such methods include the use of blowing/suction jets, a synthetic jet actuator and pulsating inlet velocity. Ravindran [5] used tangential blowing and suction through a single slot on the horizontal part of the forward facing step to control laminar flow at a flow Reynolds number of 1000. In another article, Ravindran [6] did further investigation into reduction of the reattachment length behind the backward-facing

*. *Corresponding author.*
E-mail addresses: azare@miau.ac.ir (A. Zare); hemdad@shirazu.ac.ir (H. Emdad); goshtasb@shirazu.ac.ir (E. Goshtasbi Rad)

step. Control action was achieved through the blowing of mass on the wall of the step. In these analyses, a reduced order modeling approach, suitable for active control of fluid dynamical systems based on proper orthogonal decomposition, was used. The effectiveness of this method in flow control applications is shown on a recirculation control problem behind the step using blowing or suction on the channel boundary. Jaňour and Jonáš [7] studied the effect of blowing or suction jets at the foot of the step with a momentum coefficient of 0.06 on a separated recirculation zone behind the backward facing step. Kiwan [8] investigated the localized wall discharge (blowing/suction jet) to control the recirculation zone and heat transfer characteristics downstream of a backward-facing step. The actuator was positioned on the wall opposite the step wall. Standard $k-\varepsilon$ and RNG $k-\varepsilon$ models were used for flow simulations. In the work presented by Dejoan and Leschziner [9], the effects of a periodic perturbation control strategy on step flow were investigated using Large Eddy Simulation. The controlling jet at the spanwise edge of the step, with zero-net-mass-flow rates and a Strouhal number of 0.2, was introduced into the separated shear layer flow behind a backward-facing step in a high-aspect-ratio channel. In agreement with the experimental data, results show that the computed reattachment length reduced by about 26%. In order to further investigate turbulent flow over a backward-facing step, Dejoan et al. [10] used large eddy simulation and statistical turbulence closures. A synthetic jet at the edge of the step, at an angle of 45 degrees relative to the flow direction, was introduced as a control device. Computed results showed that for a jet frequency with a Strouhal number of 0.2, the separation bubble was reduced by almost 30%. In the field of active flow control, Šaric et al. [11] studied turbulent flow over a backward-facing step. Alternative blowing/suction jets at the edge of the step were used as an actuator. Large eddy simulation, Detached eddy simulation, and transient Reynolds-averaged Navier-Stokes techniques were proposed for flow simulation. The flow Reynolds number was 3700. The periodic blowing/suction jet velocity with zero-net-mass-flux was governed by a sinusoidal law: $v_e = 0.3U_c \sin(2\pi f_e t)$, where U_c is the centerline velocity in the inlet channel. Different jet frequencies, f_e, corresponding to the Strouhal numbers ($\mathrm{St} = f_e H/U_c$) of 0.08, 0.19 and 0.30 were used as the controlling parameter. Results show that the most effective case was St=0.19.

Performing the control law on different systems, such as flow over a step in a channel, requires a large amount of CPU time and memory. Recently, low dimensional modeling by POD/Galerkin projection has received more attention as a means to overcome this problem. This method, which converts the system of an infinite dimension to a much smaller dimension, has almost the same behavior as the original system, and captures the essential dynamics of the reference system. Hence, flow control is employed for this low order model. Several researchers have investigated POD and low dimensional modeling [5,12-16]. In addition, POD has been applied for flow control purposes [5,6,15,17]. However, performing low dimensional modeling and using it in the field of flow control presents two major problems. First, the base functions or POD modes can accurately reconstruct ensembles of data that were employed in calculating POD modes. These ensembles of data are used with specific control, or without taking any controlling effects into consideration. Therefore, the reconstructed POD modes will not contain the effect of the controller. Second, the control input, such as the flow rate of blowing/suction jets, does not show up explicitly in the final low dimensional system, thus, the final system is not ready for control purposes. To handle these problems, the perturbation method on the Reynolds-Averaged Navier-Stokes equations will be introduced. The blowing/suction jet velocity, which is known as the controlling parameter, will be considered as a small perturbation on the boundary of the domain. Therefore, control parameter will appear explicitly in the reduced order model. This method is more efficient and accurate in the field of optimal control theory, with respect to other schemes based on the POD/Galerkin projection method. This paper presents an optimal technique for reducing the problem of controlling the separation bubble behind a backward facing step by injecting and extracting fluid near the step wall. It is shown that the size of the separation bubble behind the step is significantly reduced by a pair of blowing suction jets at the wall of the step.

In the following, flow simulation and the POD/Galerkin projection method are described. Then, the perturbation method and forced low dimensional model are explained. The next part explains the optimal control procedure and, finally, the results are compared with some available experimental data or numerical results. Discussion about the effectiveness of the perturbation method and controlled numerical results are presented in the last section.

2. Simulation of the turbulent flow field

2.1. Governing equations

In order to analyze turbulent flow, within reasonable CPU time consumption, over a backward-facing step in the duct, a suitable turbulence model must be chosen. In the present analysis, the Re-Normalized Group theory (RNG) $k-\varepsilon$ turbulence model [18] is used for flow simulation. The main feature of this turbulence model is its capability of capturing separation and recirculated flow fields efficiently [19].

Governing equations for incompressible flow in a Cartesian coordinate system can be described as:

Continuity equation:

$$\frac{\partial \bar{u}_i}{\partial x_i} = 0. \tag{1}$$

Momentum equation:

$$\rho\left(\frac{\partial \bar{u}_i}{\partial t} + \bar{u}_j\frac{\partial \bar{u}_i}{\partial x_j}\right) = -\frac{\partial \bar{p}}{\partial x_i} + \frac{\partial}{\partial x_j}\left(\tau_{ij}^L - \rho\overline{u_l'u_J'}\right). \tag{2}$$

Here, τ_{ij}^L is the laminar (molecular) constituent of the stress tensor defined by:

$$\tau_{ij}^L = \mu\left(2S_{ij} - \frac{2}{3}\frac{\partial \bar{u}_k}{\partial x_k}\delta_{ij}\right), \tag{3}$$

and S_{ij} is the strain rate tensor given by:

$$S_{ij} = \frac{1}{2}\left(\frac{\partial \bar{u}_i}{\partial x_j} + \frac{\partial \bar{u}_j}{\partial x_i}\right). \tag{4}$$

Using the Boussinesq approximation [20], the turbulent stress tensor appears as:

$$-\rho\overline{u_l'u_J'} = \mu_t\left(2S_{ij} - \frac{2}{3}\frac{\partial \bar{u}_k}{\partial x_k}\delta_{ij}\right) - \frac{2}{3}\rho k\delta_{ij}. \tag{5}$$

μ_t is the turbulent viscosity defined by the RNG $k-\varepsilon$ turbulence model. The last term within the turbulent stress tensor plays a role similar to that of the pressure in the total laminar stress tensor. Therefore, this term will be referred to as the turbulent pressure and denoted as $p_T = 2/3\rho k$.

Turbulent kinetic energy [18]:

$$\frac{\partial \rho k}{\partial t} + \frac{\partial}{\partial x_i}\left(\rho\bar{u}_i k - \frac{\mu_{\text{eff}}}{\sigma_k}\frac{\partial k}{\partial x_i}\right) = \mu_t S^2 - \rho\varepsilon. \tag{6}$$

Dissipation rate [18]:

$$\frac{\partial \rho\varepsilon}{\partial t} + \frac{\partial}{\partial x_i}\left(\rho\bar{u}_i\varepsilon - \frac{\mu_{\text{eff}}}{\sigma_\varepsilon}\frac{\partial \varepsilon}{\partial x_i}\right) = C_{1\varepsilon}\mu_t S^2\frac{\varepsilon}{k} - C_{2\varepsilon}\rho\frac{\varepsilon^2}{k} - R', \tag{7}$$

$$\mu_{\text{eff}} = \mu_t + \mu \quad \text{and} \quad S = \sqrt{2S_{ij}S_{ij}}.$$

Turbulent viscosity:

$$\mu_t = \frac{\rho c_\mu k^2}{\varepsilon}. \tag{8}$$

R' in Eq. (7) is defined as: $R' = \frac{c_\mu\rho\eta^3(1-\eta/\eta^\circ)}{1+\beta\eta^3}\frac{\varepsilon^2}{k}$, $\eta = Sk/\varepsilon$, $\eta^\circ = 4.83$, and $\beta = 0.012$ [18]. The other experimental constants are: $c_\mu = 0.0845$, $c_{1\varepsilon} = 1.42$, $c_{2\varepsilon} = 1.68$, $\sigma_k = \sigma_\varepsilon = 0.718$.

Variables with the over bar "-" are the time averaged values. Hereafter, for the sake of simplicity, the over bar on dependent variables will be omitted.

2.2. Computational domain and boundary conditions

The computational domain and boundaries of this study are illustrated in Figure 1. The computational domain extends to $l = 30H_s$ upstream of the step. The outlet boundary should be far enough ($L \approx 4x_r$, where x_r is a reattachment length) that the results will be independent of the outlet boundary position. Step height is $H_s = 1$ and duct height is $H = 2H_s$. The boundary conditions over this geometry are as follows:

(1) At the inflow boundary, Γ_{in}, a constant normalized velocity of $u = 1.0$ and $v = 0.0$ is imposed. For k and ε, a constant value of 0.01 and 0.05 is used.

(2) At the out-flow boundary, Γ_{out}, the outflow condition is specified (zero gradients of each flow variable in the streamwise direction are considered).

(3) On the solid walls, Γ_{wall}, a no slip condition ($u = 0.0$ and $v = 0.0$) is imposed. Values of k and ε for the first grid point near the walls are predicted by the standard wall function. y^+near the walls ($y^+ = yu_\tau/v$ where u_τ is the friction velocity) is taken to be more than 30. The boundary

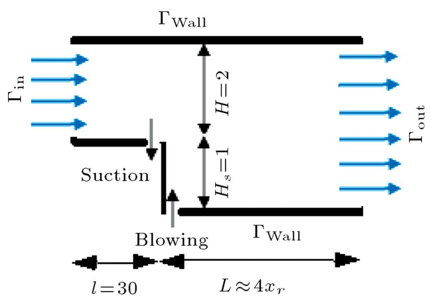

C1 (blowing/suction jets at the foot and edge of the step)

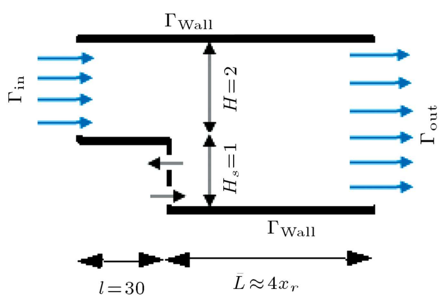

C2 (blowing/suction jets at the wall of the step, blowing at foot and suction at 0.7H$_s$)

Figure 1. The computational domain

conditions for k and ε on the walls are: $\partial k/\partial n = 0$ and $\partial\varepsilon/\partial n = 0$, where n is the normal coordinate to the wall.

(4) For the surface actuation, two different controlling cases are considered (see Figure 1):

- **Case C1:** Blowing/suction jets are at the foot and edge of the step with tangential and normal velocities of $(u, v) = (0, \pm\varepsilon_p)$;
- **Case C2:** Blowing/suction jets are at the step wall, blowing at the foot of the step, and suction at $0.7H_s$, with tangential and normal velocities of $(u, v) = (\pm\varepsilon_p, 0)$.

The governing equations (Eqs. (1)-(8)) are solved on a staggered grid system using the finite volume method with the SIMPLE algorithm [21]. The non-dimensional equations are transformed into a curvilinear coordinate system. The conservation laws are integrated over a control volume, and the Gauss theorem is used to transform volume integrals into surface integrals. The power law scheme is used in discretizing convective terms of the governing equations. Diffusion terms are discretized by central differencing. The unsteady state flow field is obtained by solving flow equations for each time step.

3. Reduced order system

3.1. Review of classical proper orthogonal decomposition/Galerkin projection

POD and Galerkin projection are tools for producing reduced order systems from the large data sets. The central idea of POD is to obtain a subspace of the large data sets in such a way that it optimally spans the data. In other words, error in the projection of the data onto the subspace of the POD modes is minimized. Details and fundamentals of POD can be found in Berkooz et al. [12]. In performing POD modes, it is necessary to solve an eigenvalue problem as:

$$\int_\Omega R(x,\xi)\varphi_n d\xi = \lambda_n \varphi_n(x) \qquad n = 1, 2, ..., \tag{9}$$

$R(x, \xi)$ is a two point correlation that must be produced from the experimental or numerical data sets, x and ξ are vector coordinates of two points in the domain of Ω. λ_n and φ_n are eigenvalues and orthonormal eigenfunctions, respectively, and n is the number of modes. Numerical simulation of the fluid flow is available at m discrete grid points and n different times. In this case, $R(x, \xi)$ is replaced with a matrix $P_{ij} = 1/n \sum_{k=1}^{n} u(x_i, t_k)\, u(x_j, t_k)$, $i, j = 1, 2, ..., m$ and the eigenvalue problem based on Eq. (9) is reduced to finding eigenvalues and eigenfunctions of the P matrix. Solving the eigenvalue problem for the $m \times m$ matrix over the computational domain is intensive, and the method using snapshots, which was introduced by Sirovich [22], can be used. Based on this method, it suffices to solve the n-dimensional eigenvalue problem, where n is the number of snapshots. The eigen system takes the form:

$$U\omega_i = \lambda_i \omega_i, \tag{10}$$

where the correlation matrix, U, is defined as:

$$U_{ij} = \frac{1}{n}(\mathbf{u}_i, \mathbf{u}_j) \quad i, j = 1, 2, ..., n$$

$$\mathbf{u}_i = [\mathbf{u}(x_1, t_i) \ \cdots \ \mathbf{u}(x_m, t_i)]. \tag{11}$$

U is a non-negative Hermitian matrix, so it has a complete set of orthogonal eigenvectors, ω_i. Thus, the POD mode is assumed to be a linear combination of the data vectors:

$$\varphi_1 = \sum_{i=1}^{n} \omega_i^1 u_i \quad \varphi_2 = \sum_{i=1}^{n} \omega_i^2 u_i \quad \cdots \quad \varphi_n = \sum_{i=1}^{n} \omega_i^n u_i. \tag{12}$$

For the inner product $\langle ., . \rangle$, it is now easy to check:

$$\langle \varphi_i, \varphi_j \rangle = \begin{cases} 1 & i = j \\ 0 & i \neq j \end{cases} \tag{13}$$

See [6] for details.

Once the POD modes are obtained, as described here, the velocity vector at any specific instance can be reconstructed by POD modes as:

$$\mathbf{u}(\mathbf{x}, t) = \sum_{j=1}^{n} a_j(t) \boldsymbol{\varphi}_j(\mathbf{x}), \tag{14}$$

where, $a_j(t)$ is the time dependent coefficient of the POD decomposition and $\boldsymbol{\varphi}_\mathbf{j}(\mathbf{x})$ is the vector of POD modes.

It is also customary to remove the average value, $\mathbf{u}^*$, from snapshots prior to calculation of the POD modes:

$$\mathbf{u}(\mathbf{x}, t) = \mathbf{u}^* + \sum_{j=1}^{n} a_j(t) \boldsymbol{\varphi}_\mathbf{j}(\mathbf{x}). \tag{15}$$

The reduced order model is developed by Galerkin projection on the Reynolds-Averaged Navier-Stokes (RANS) equations. Consider the following dynamical system, which is governed by the Time-Averaged incompressible Navier-Stokes equations in non-dimensional form:

$$\frac{\partial \mathbf{u}}{\partial t} = -\boldsymbol{\nabla} p + L_1(\mathbf{u}) + Q(\mathbf{u}, \mathbf{u}) + L_2(\mathbf{u}), \tag{16}$$

where, L_1 and Q are linear and quadratic bilinear operators, respectively:

$$L_1(\mathbf{u}) = \frac{1}{\mathrm{Re}}\boldsymbol{\nabla}^2\mathbf{u},$$

$$Q(\mathbf{u},\mathbf{u}) = -(\mathbf{u}.\boldsymbol{\nabla})\mathbf{u},$$

and :

$$L_2(\mathbf{u}) = \boldsymbol{\nabla}.\left(\frac{\mu_t^*}{\mathrm{Re}}(\boldsymbol{\nabla}\mathbf{u} + \boldsymbol{\nabla}\mathbf{u}^T)\right).$$

μ_t^* is non-dimensional turbulent viscosity, and p is a combination of the pressure term and turbulent pressure, $p_T = 2/3\rho k$.

Substituting Eq. (15) into the RANS equations and taking the inner product of the resultant equation, with respect to $\boldsymbol{\varphi}_i$, the set of nonlinear Ordinary Differential Equations (ODEs) is obtained as a result of the orthonormal property of the POD modes:

$$\dot{a}_i = \langle \mathbf{R}, \boldsymbol{\varphi}_i\rangle,$$

$$\mathbf{R} = L_1(\mathbf{u}) + L_2(\mathbf{u}) + Q(\mathbf{u},\mathbf{u}) - \boldsymbol{\nabla}p. \tag{17}$$

The inner product is defined as:

$$\langle \mathbf{c}_1, \mathbf{c}_2\rangle = \int_\Omega \mathbf{c}_1(x).\mathbf{c}_2(x)d\Omega. \tag{18}$$

An important property of orthonormal POD mode functions is that, if every snapshot satisfies a given linear constraint, then, the POD modes will satisfy that constraint also. An example of that constraint is the divergence free condition for velocity in incompressible flow. Therefore, for incompressible flow, using the divergence free property of the POD modes, the pressure term can be reduced to [14]:

$$\langle \boldsymbol{\nabla}p, \boldsymbol{\varphi}_i\rangle = \int_\Omega \boldsymbol{\varphi}_i.\boldsymbol{\nabla}p d\Omega = \int_\Omega \mathrm{div}(p\boldsymbol{\varphi}_i)d\Omega$$

$$= \int_{\partial\Omega} p\boldsymbol{\varphi}_i.\mathbf{n}ds. \tag{19}$$

The main advantage of Eq. (14) is that the pressure term will be needed solely on the boundary of the domain, $\partial\Omega$, and for zero velocity and zero mode function on the boundary, the pressure term in Eq. (17) will vanish. Finally, after some manipulations, the reduced order system (Eq. (17)) can be written as follows:

$$\dot{a}_i = \alpha_i + \beta_{ij}a_j + \gamma_{ijk}a_j a_k, \tag{20}$$

where:

$$\alpha_i = \langle L_1(\mathbf{u}^*) + L_2(\mathbf{u}^*) + Q(\mathbf{u}^*,\mathbf{u}^*), \boldsymbol{\varphi}_i\rangle,$$

$$\beta_{ij} = \langle L_1(\boldsymbol{\varphi}_j) + L_2(\boldsymbol{\varphi}_j) + Q(\mathbf{u}^*,\boldsymbol{\varphi}_j) + Q(\boldsymbol{\varphi}_j,\mathbf{u}^*), \boldsymbol{\varphi}_i\rangle,$$

$$\gamma_{ijk} = \langle Q(\boldsymbol{\varphi}_k,\boldsymbol{\varphi}_j), \boldsymbol{\varphi}_i\rangle.$$

3.2. Introducing perturbation method

Eq. (20) is in the state space format, which is applicable for control purposes. However, this set of equations is autonomous and the effect of the actuator is still buried in the boundary conditions. Besides, the POD modes are obtained without any controlling effects. In this section, the perturbation method proposed to remedy these problems is investigated. Considering control input as a small perturbation in the boundary conditions, the objective is to find the resulting changes in the flow due to these disturbances. Let us perturb the dependent variables by ε_p:

$$\mathbf{u} = \mathbf{u}_o + \varepsilon_p\mathbf{u}_1,$$

$$p = p_o + \varepsilon_p p_1, \tag{21}$$

where variables with subscripts "o" and "1" are the time averaged flow variables without any control input (or with a specific controller) and with controlling effects, respectively. It is important to notice that the simple step or impulse controlling jet is inserted on the boundary conditions of the perturbation equations and ε_p is introduced as the perturbation parameter. Substituting the perturbed flow variables in the incompressible Time-Averaged Navier-Stokes equations and ignoring terms with powers of ε_p greater than one, the following equations will be obtained:

$$\boldsymbol{\nabla}.(\mathbf{u}_o + \varepsilon_p\mathbf{u}_1) = 0,$$

$$\begin{aligned}\frac{\partial(\mathbf{u}_o + \varepsilon_p\mathbf{u}_1)}{\partial t} = &- \boldsymbol{\nabla}(p_o + \varepsilon_p p_1) + \frac{1}{\mathrm{Re}}\boldsymbol{\nabla}^2(\mathbf{u}_o + \varepsilon_p\mathbf{u}_1)\\ &+ \boldsymbol{\nabla}.\left(\frac{\mu_t}{\mathrm{Re}}(\boldsymbol{\nabla}(\mathbf{u}_o + \varepsilon_p\mathbf{u}_1)\right.\\ &\left.+ \boldsymbol{\nabla}(\mathbf{u}_o + \varepsilon_p\mathbf{u}_1)^T)\right) - (\mathbf{u}_o.\boldsymbol{\nabla})\mathbf{u}_o\\ &- \varepsilon_p(\mathbf{u}_o.\boldsymbol{\nabla})\mathbf{u}_1 - \varepsilon_p(\mathbf{u}_1.\boldsymbol{\nabla})\mathbf{u}_o.\end{aligned} \tag{22}$$

The coefficients of the power of $\varepsilon_p^o(\varepsilon_p^o = 1)$ and $\varepsilon_p^1(\varepsilon_p^1 = \varepsilon_p)$ should be set equal to zero, since they are linear independent. Therefore, two sets of equations will be obtained.

1) Uncontrolled time-averaged Navier-Stokes equations, which are labelled as equations A:

$$\boldsymbol{\nabla}.\mathbf{u}_o = 0$$

$$\begin{aligned}\frac{\partial\mathbf{u}_o}{\partial t} = &- \boldsymbol{\nabla}p_o + \frac{1}{\mathrm{Re}}\boldsymbol{\nabla}^2\mathbf{u}_o\\ &+ \boldsymbol{\nabla}.\left(\frac{\mu_t}{\mathrm{Re}}(\boldsymbol{\nabla}\mathbf{u}_o + \boldsymbol{\nabla}\mathbf{u}_o^T)\right) - (\mathbf{u}_o.\boldsymbol{\nabla})\mathbf{u}_o.\end{aligned} \tag{23}$$

2) Time-averaged linear perturbation equations, which are labelled as equations B:

$$\begin{aligned}&\boldsymbol{\nabla}.\mathbf{u}_1 = 0\\&\frac{\partial \mathbf{u}_1}{\partial t} = -\boldsymbol{\nabla} p_1 + \frac{1}{\mathrm{Re}}\boldsymbol{\nabla}^2\mathbf{u}_1\\&\qquad + \boldsymbol{\nabla}.\left(\frac{\mu_t}{\mathrm{Re}}(\boldsymbol{\nabla}\mathbf{u}_1 + \boldsymbol{\nabla}\mathbf{u}_1^T)\right)\\&\qquad - (\mathbf{u}_o.\boldsymbol{\nabla})\mathbf{u}_1 - (\mathbf{u}_1.\boldsymbol{\nabla})\mathbf{u}_o. \end{aligned}\tag{24}$$

The set of equations A are the incompressible nonlinear RANS equations governed by the uncontrolled flow field (or flow field with specific control input), and they will be solved with the RNG $k-\varepsilon$ turbulence model. Besides, the set of linear equations B is calculated based on the solution of the set of equations A. The control inputs will be imposed on the boundary conditions of the perturbed equations. In addition, a turbulent model should be used in solving the set of equations B. Here, the RNG $k-\varepsilon$ equations are not perturbed. Actually, they will be solved in each iteration process of the solution algorithm. This will cause the effect of the blowing/suction jet on flow turbulence to be considered in μ_t (turbulent viscosity coefficient). It is noteworthy that μ_t will be solely timed to the perturbation velocity (Eq. (24)). Therefore, the effect of the new μ_t with blowing/suction will not be considered on the RANS equations (Eq. (23)). Turbulent flow separation over the backward-facing step is controlled by a pair of blowing/suction jets, and the jet velocity on the solid walls is introduced as a control input. The value of the control inputs or the velocity of the blowing/suction jets are not known at this stage and, because of the linearity of the set of equations B, a simple step or impulse can be used as a control input. Finally, the full controlled flow field can be estimated based on Eq. (21). The accuracy of the perturbation method is investigated for the turbulent flow over a backward-facing step at different flow Reynolds numbers of 20000 and 44000 (see Section 5.2).

3.3. Forced reduced order model

If $\{\boldsymbol{\varphi}_j \in H | j = 1,2,...,n\}$ are POD modes calculated by POD analysis of the ensembles $\{\mathbf{u}_o(\mathbf{x},t_k) \in H | k = 1,...,n\}$ with averaged values of $\mathbf{u}^*$, the velocity field, considering the effects of the control inputs from a pair of blowing/suction controlling jets, can be expanded as:

$$\mathbf{u}(\mathbf{x},t) = \mathbf{u}^*(\mathbf{x}) + \sum_{j=1}^{n} a_j(t)\boldsymbol{\varphi}_j(\mathbf{x}) + \varepsilon_p \mathbf{u}_1(\mathbf{x},t). \tag{25}$$

$\mathbf{u}_1(\mathbf{x},t)$ is the response of the set of equations B to impulse input as a boundary control input. Substituting Eq. (25) into flow field equations (RANS equations) and taking the inner product, with respect to the mode function, $\boldsymbol{\varphi}_i$, the non-autonomous forced low dimensional model will be obtained because of the orthonormal property of the POD mode functions:

$$\dot{a}_i = \alpha_i + \beta_{ij}a_j + \gamma_{ijk}a_ja_k + \theta_i\varepsilon_p + \rho_{ij}a_j\varepsilon_p, \tag{26}$$

where:

$$\begin{aligned}&\alpha_i = \langle L_1(\mathbf{u}^*) + L_2(\mathbf{u}^*) + Q(\mathbf{u}^*,\mathbf{u}^*), \boldsymbol{\varphi}_i\rangle,\\&\beta_{ij}=\langle L_1(\boldsymbol{\varphi}_j)+L_2(\boldsymbol{\varphi}_j)+Q(\mathbf{u}^*,\boldsymbol{\varphi}_j)+Q(\boldsymbol{\varphi}_j,\mathbf{u}^*),\boldsymbol{\varphi}_i\rangle,\\&\gamma_{ijk} = \langle Q(\boldsymbol{\varphi}_k,\boldsymbol{\varphi}_j),\boldsymbol{\varphi}_i\rangle,\\&\theta_i=\langle L_1(\mathbf{u}_1)+L_2(\mathbf{u}_1)+Q(\mathbf{u}^*,\mathbf{u}_1)+Q(\mathbf{u}_1,\mathbf{u}^*)-\dot{\mathbf{u}}_1,\boldsymbol{\varphi}_i\rangle,\\&\rho_{ij} = \langle Q(\mathbf{u}_1,\boldsymbol{\varphi}_j) + Q(\boldsymbol{\varphi}_j,\mathbf{u}_1),\boldsymbol{\varphi}_i\rangle.\end{aligned}$$

In these nonlinear ODEs, the controlling input or perturbation parameter, ε_p, appears as the coefficient of the terms θ_i and ρ_{ij}, and optimal control theory can be applied to these equations. Obviously, based on the perturbation method, two sets of ensembles, $\{\mathbf{u}_o(\mathbf{x},t_k)\}$ and $\{\mathbf{u}_1(\mathbf{x},t_k)\}$, should be gathered in performing the control procedure.

4. Optimal control

The blowing/suction jet velocity is the controlling parameter, which is presented as ε_p in the forced low dimensional model (Eq. (26)). The control problem is to find the time variation of ε_p on a specific time interval, $[t_o,t_f]$, in such a way that cost function, J, [15] is minimized:

$$J = \frac{1}{2}\int_{t_o}^{t_f}\left(\int_\Omega \zeta^2 d\Omega + R\varepsilon_p^2\right)dt, \tag{27}$$

where, ζ is the vorticity and R is a positive constant regarding the control input, ε_p. The vorticity field can be expanded by mode functions:

$$\zeta = \sum_{i=1}^{n} a_i(t)\zeta_i(x), \tag{28}$$

where, ζ_i is the vorticity of the ith mode and a_i is the coordinates of ζ in subspace S. After substituting Eq. (28) into the cost function equation, J, Eq. (27) reduces to:

$$J = \frac{1}{2}\int_{t_o}^{t_f}\left(a^TQa + \varepsilon_p^T R\varepsilon_p\right)dt, \tag{29}$$

where:

$$\int_\Omega \zeta_i\zeta_j d\Omega = Q_{ij}. \tag{30}$$

Optimal control of the forced low dimensional model can be performed by introducing the Hamiltonian functional [23]. The Hamiltonian functional comprises a reduced order model (Eq. (26)) and index function (Eq. (29)). By differentiating the Hamiltonian functional, the state, co-state and stationary condition equations will be obtained. The perturbation parameter, ε_p, is derived from the linear algebraic stationary condition equation:

$$\varepsilon_p = \xi_i \lambda_i + \mu_{ij} \lambda_i a_j, \tag{31}$$

where:

$$\xi_i = -\frac{\theta_i}{2R},$$

$$\mu_{ij} = -\frac{\rho_{ij}}{2R}.$$

After performing some manipulations on the state, costate and stationary condition equations, the nonlinear set of ODEs, which govern the optimal behaviors of the forced reduced order system, will be obtained:

$$\begin{aligned} \dot{a}_i =& \alpha_i + \beta_{ij} a_j + \gamma_{ijk} a_j a_k + \theta_i \xi_j \lambda_j + \theta_i \mu_{hj} \lambda_h a_j \\ &+ \rho_{ij} \xi_k \lambda_k a_j + \rho_{ij} \mu_{kh} \lambda_k a_j a_h, \\ \dot{\lambda}_i =& (Q_{ij} + Q_{ji})\, a_j + \beta_{ij} \lambda_j + (\gamma_{kji} + \gamma_{kij}) a_j \lambda_k \\ &+ \rho_{ki} \xi_k \lambda_k \lambda_j + \rho_{ki} \mu_{lj} \lambda_l a_k \lambda_k. \end{aligned} \tag{32}$$

The initial conditions are:

$$a(t = t_o) = a_o,$$

$$\lambda(t = t_f) = 0.0. \tag{33}$$

λ_i is the ith costate variable or Lagrange multiplier. These sets of equations are nonlinear with split initial conditions. The method of Quasi-linearization of Kirk [23] in an iterative manner will be used to solve them (see Appendix A). Finally, the value of ε_p will be computed at the time interval, $\Delta t^* > \Delta t$ (Δt is the time step size of flow simulation), for each positive value of constant R in Eq. (27). In the following, the step by step procedure of calculating ε_p and the flowchart of the control procedure (Figure 2) at each time interval, Δt^*, are given.

i. Computing the snapshots $\{\mathbf{u}_o(\mathbf{x}, t_k)\}$ by solving RANS equations with a RNG $k-\varepsilon$ model without any control input (or with specific controller), and calculating POD modes by solving an eigenvalue problem;

ii. Setting the index of time step i to 1 ($i = 1$) and letting $\varepsilon_{pi} = 1$;

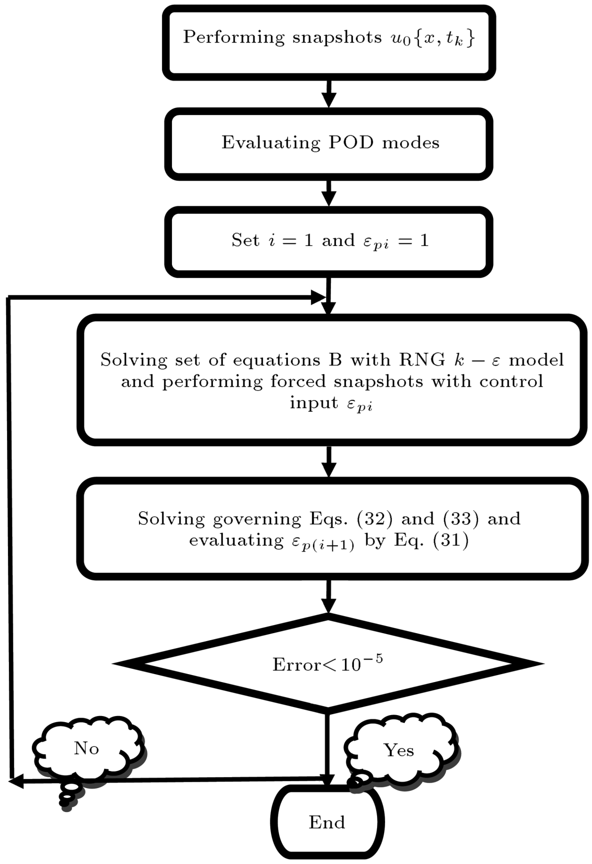

Figure 2. Feedback control procedure.

iii. Computing snapshots $\{\mathbf{u}_1(\mathbf{x}, t_k)\}$ by solving the perturbed RANS equations (set of equations B) with the RNG $k-\varepsilon$ turbulent model, and control input parameter, ε_{pi}, set as a boundary condition;

iv. Solving the set of Eq. (32) and (33) by the quasi-linearization algorithm of Kirk [23] and calculating a new value for $\varepsilon_{p(i+1)}$ (Eq. (31));

v. If error $= |\varepsilon_{pi+1} - \varepsilon_{pi}| \leq 10^{-5}$, the iterative procedure has converged and goes to step vi, otherwise add 1 to i and go to step iii;

vi. The procedure is completed and the control input parameter is obtained.

5. Example: Turbulent flow over backward-facing step

5.1. Validation of the fluid flow simulation code

The veracity of the developed SIMPLE code is examined by computing the flow field over a backward-facing step at the flow Reynolds number of 44000. The numerical results should be independent of grid size. Therefore, different grid distributions are studied (see Figure 3). Based on a grid independency check, the computational domain is discretized by 199×53 grid points. The computed reattachment length by this grid is estimated as $x_r = 7H_s$, while Kim et al. [24] reported it as between $6.5H_s$ and $7.5H_s$ (H_s is step height). Comparison of the predicted velocity profile with the experimental results of Kim et al. [24] at different distances of $x = 2.66$, 5.33, 6.22 and 8.00 from the step position is presented in Figure 4. Results show that RNG $k-\varepsilon$ code developed in this article has good agreement with experimental results. In these calculations, y^+ near the walls ($y^+ = (yu_\tau/v$ where u_τ is the friction velocity) is taken to be more than 30.

5.2. Accuracy of the perturbation method on the RANS equations

In order to investigate the accuracy of the perturbation method, a steady state turbulent flow over a backward-facing step is simulated by two different methods. For both methods, the flow Reynolds number is taken to be 20000 and 44000, and a pair of blowing/suction jets is introduced as a controller.

Method i: RANS equations are solved with the RNG $k-\varepsilon$ turbulent model, and a pair of blowing/suction jets with constant velocity of ε_p is used as controller. (Cases C1 and C2 presented in Figure 1 are investigated.)

Method ii: At first, RANS equations with the RNG $k-\varepsilon$ turbulent model (Eq. (23)) without any controller (Case C1) or with a specific controlling jet (Case C2) are solved. Then, the perturbed flow equations (Eq. (24)) are solved with a pair of blowing/suction controlling jets with constant velocity of one (perturbed flow equations are solved with the RNG $k-\varepsilon$ turbulent model). The resulting flow field, with a different controlling jet velocity of ε_p, is computed using Eq. (21).

X-velocity profiles near the lower wall of the step, at $y = 0.04$ and $0 \le x \le 40$, for different perturbation parameters of $\varepsilon_p = 0.1$ and 0.5 for Case C1, and flow Reynolds numbers of 20000 and 44000, are presented in Figure 5. Results of the perturbation method (Method ii) are in good agreement with flow simulations based on the RANS equations and the reattachment length is estimated properly. It should be noted that as the perturbation parameter grows, the deviation of the flow field between the two methods is more pronounced. Still, the results are good enough for the purpose of the control procedure, with respect to the existing methods in which the effect of a controller on the flow field is not taken into account.

For Case C2, the set of equations A is solved with a specific controlling jet $(u, v) = (\pm 1, 0)$. X-velocity profiles at $y = 0.04$ near the lower wall of the step are simulated by Methods (i) and (ii) for perturbation parameters of $\varepsilon_p = 0.5$, 1, 1.5 and 2, which are presented in Figure 6. Computational results show good agreement between the RANS solution and the perturbation method. It can be concluded that the perturbation method with controlling jets on the wall of the step is more efficient in predicting the flow

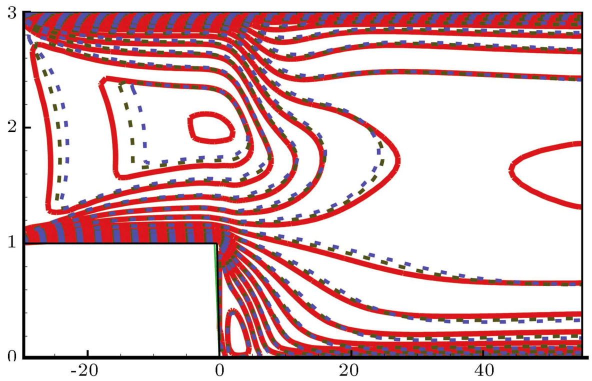

Figure 3. x-velocity contours with different grid distributions. Solid line: 199 × 53 grid points; dashed line: 209 × 80 grid points, and dashed-doted line 299 × 100 grid points.

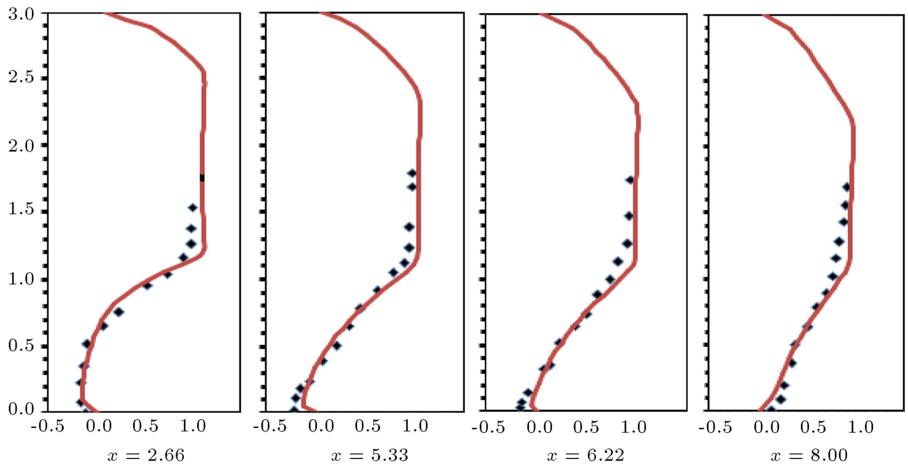

Figure 4. Comparison of numerical and experimental values of x-velocity profiles at different locations. (♦ Experimental results of Kim et al. [24], — present numerical results).

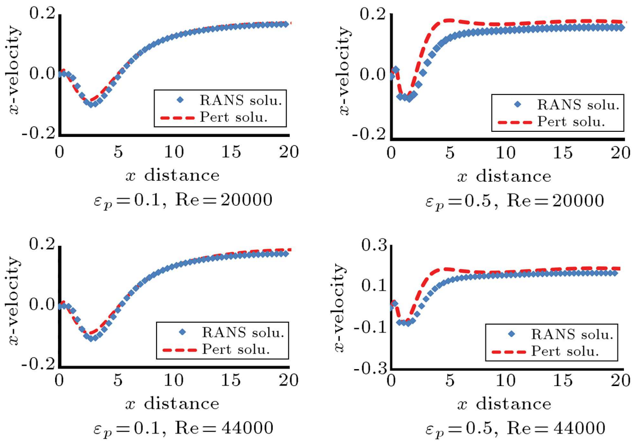

Figure 5. Comparison of the x-velocity profiles computed by different methods for Case C1. ♦ Method i and - - - Method ii.

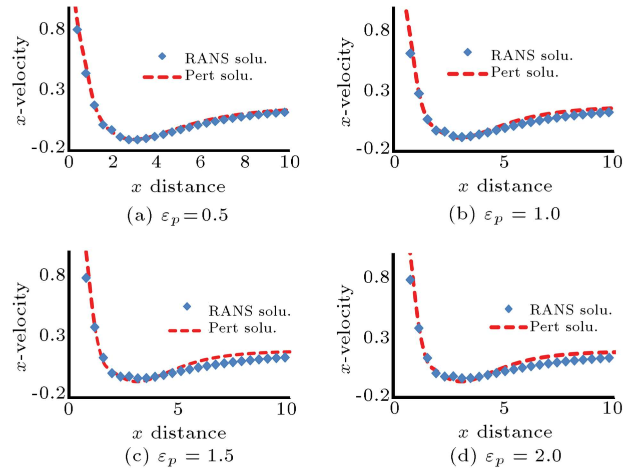

Figure 6. Comparison of the x-velocity profiles computed by different methods for Case C2. ♦ Method i and - - - Method ii.

field over the step. This is mainly due to the smaller separation zone, with respect to Case C1.

5.3. *Flow simulation by POD/Galerkin projection method*

Unsteady turbulent flow over a backward-facing step at a Reynolds number of 44000 is estimated by solving RANS equations with the RNG $k-\varepsilon$ turbulent model. The time step size is taken to be $\Delta t = 0.005$. POD is carried out on 40 snapshots of the solutions obtained by simulating the Reynolds Averaged Navier-Stokes system in the nondimensional time interval [4.8,5]. Eigenvalues that represent the average energy of snapshots gained by each base function are presented in Figure 7. The x-velocity contours reconstructed by 40 POD modes for a specific snapshot at a non-dimensional time of $t = 5$ are compared with the RANS solution in Figure 8(a) and (b) presents the comparison of x-velocity contours reconstructed by 5 POD modes. As shown in this figure, a good agreement with the

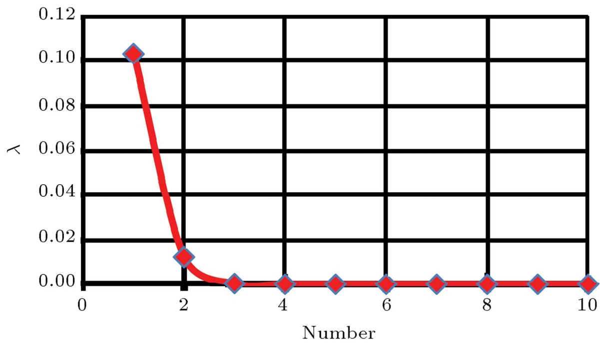

Figure 7. Variation of the eigenvalues.

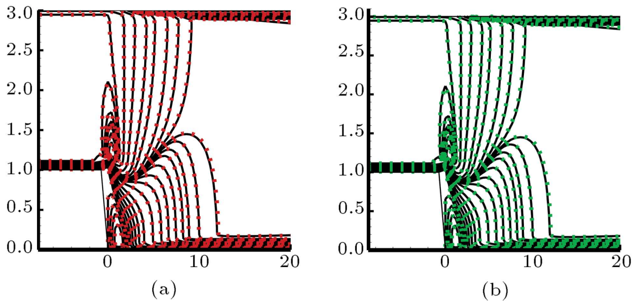

Figure 8. Comparison of the x-velocity contours. Solid line: RANS solution and dashed line: POD analysis at non-dimensional time $t = 5$: (a) 40 POD modes; and (b) 5 POD modes.

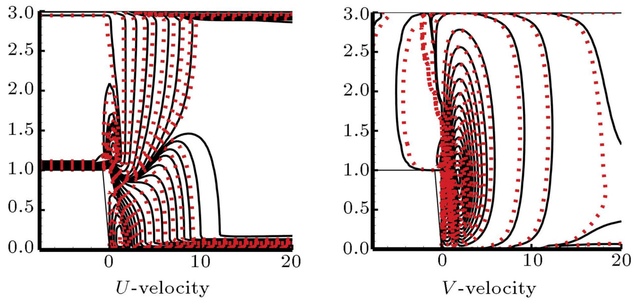

Figure 9. Comparison of the x and y-velocity contours. Solid line RANS solution and dashed line: POD analysis at non-dimensional time $t = 4.9$.

RANS solution for 5 POD modes is also achieved. The results show that different cases with 40 and 5 POD mode functions estimate the turbulent flow field over a step accurately. In order to study the accuracy of the POD/Galerkin projection method, the POD modes with 40 snapshots in the non-dimensional time interval [4,4.2] are generated to obtain the flow field at a non-dimensional time of 4.9. The obtained results are in good agreement with the RANS solution, as shown in Figure 9.

In order to study the stability of the reduced order model, the evolution of the time coefficients, a_1 and a_2, of the first two POD modes at non-dimensional time interval [0,5] are shown in Figure 10. As is apparent, the time-dependent coefficients asymptote to a constant steady-state value as time increases, and COR tends to 1 as time increases.

Root Mean Square Error (RMSE) and correlation coefficients (COR) are defined as:

$$\mathrm{RMSE} = \sqrt{\frac{\sum_{i=1}^{\mathrm{ng}} (u_i - u_{\mathrm{podi}})^2}{\mathrm{ng}}}, \tag{34}$$

$$\mathrm{COR} = \frac{\sum_{i=1}^{\mathrm{ng}} (u_i - \bar{u})(u_{\mathrm{podi}} - \overline{u_{\mathrm{pod}}})}{\sqrt{\sum_{i=1}^{\mathrm{ng}} (u_i - \bar{u})^2}\sqrt{\sum_{i=1}^{\mathrm{ng}} (u_{\mathrm{podi}} - \overline{u_{\mathrm{pod}}})^2}}, \tag{35}$$

where, ng is the number of grid points and u_i and u_{podi} are RANS and POD reduced order model solutions, respectively. $\bar{u}$ and $\overline{u_{\mathrm{pod}}}$ are time averaged solutions corresponding to the RANS solution, and POD reduced order model results over non-dimensional time interval [0,5]. The RMSE and COR between the RANS solution and the reconstructed flow field by POD/Galerkin projection are presented in Figure 11. It is clear that RMSE is reduced and that COR reached 1 as time increased.

5.4. Flow control results

Reduction of the reattachment length or removing the separation bubble is the main goal of the flow control over a backward-facing step. In this article, a flow Reynolds number of 44000 is investigated. To simulate the performance of the controller, two sets of snapshots

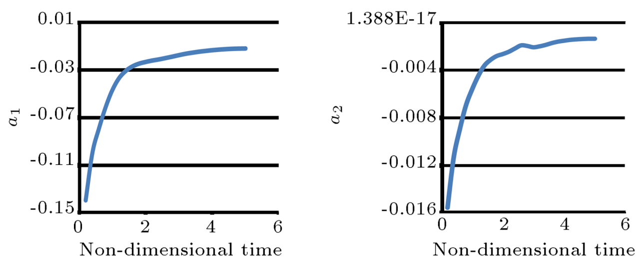

Figure 10. Evolution of the time coefficients a_1 and a_2.

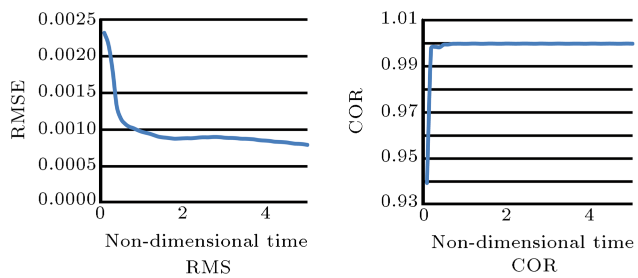

Figure 11. Variation of RMS and COR with respect to non-dimensional time.

should be taken; one from the solution of RANS equations with the RNG $k-\varepsilon$ turbulent model, with zero controlling affects for Case C1, and with a constant jet velocity of one for Case C2 (hereafter referred to as unforced snapshots). The next snapshots are taken from the solution of the perturbed RANS equations with the RNG $k-\varepsilon$ turbulent model (Eq. (24)). A control input with constant jet velocity of 1 is introduced in the boundary condition of the perturbed flow equations. They will be called forced snapshots. Forty snapshots for each set of equations A and B are taken in the time interval of $\Delta t^* = 1$. A pair of blowing/suction jets is introduced as controlling jets. At first, the POD modes are calculated based on unforced snapshots. Then, the unknown parameters, such as α_i, β_{ij} and γ_{ijk} in Eq. (26), are computed. The parameters, θ_i and ρ_{ij}, are obtained by forced snapshots. Substituting the results into Eq. (32), the resulting equations are solved by the quasi-linearization algorithm of Kirk [23] (The algorithm is presented in Appendix A). Finally, the perturbation parameter, ε_p, is computed for each time interval, Δt^*, by Eq. (31). This procedure is repeated until the specific value for the perturbation parameter is obtained. In this study, two different controlling devices are investigated, namely, Cases C1 and C2 (see Figure 1). The selection of the position for blowing/suction jets is crucial for the effectiveness of the control. Here, controlling results for Cases C1 and C2 and the effects of controlling jets on the reattachment length behind the backward-facing step are discussed.

Case C1: Here, we analyze the controlling results of the blowing/suction jets at the foot and edge of the step. The perturbation parameter or blowing/suction controlling jet velocity variation, with respect to time, for different values of positive constant R (Eq. (29)), is presented in Figure 12. Control input or jet velocity becomes larger with time as the separation bubble grows and becomes constant after transient effects decay. The sensitivity of the flow control problem is analyzed for a different number of snapshots, such as 10, 20 and 40, in Figure 13. It is obvious that for a different number of snapshots for specific time interval Δt^* and positive constant R, the results are similar, and jet velocity becomes larger as the separation region grows. Values of the reattachment length, with and without control, for different values of the positive constant R are listed in Table 1. Results show that controlling jets perform better as positive

Table 1. Reattachment length with and without control for different values of the positive constant R (Case C1).

R	2.0×10^{-6}	$1.0\times10^{-}6$	9.0×10^{-7}	8.0×10^{-7}	No control
x_r	6.76	5.07	4.35	3.14	6.95
Reduction	2.7%	27%	37%	54%	—

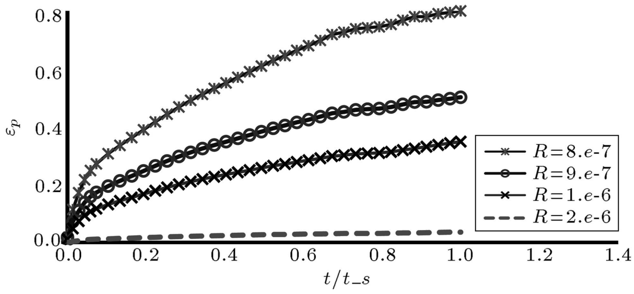

Figure 12. Control input variation with respect to time for different values of positive constant of R for Case C1 (t_s is a time of steady state flow).

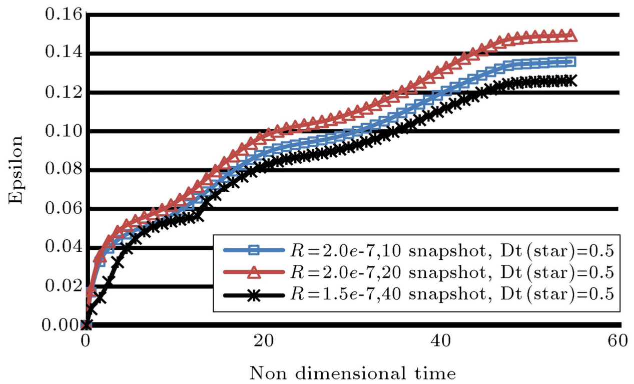

Figure 13. Control input variation with respect to time for specific value of Δt^* and different number of snapshots for Case C1.

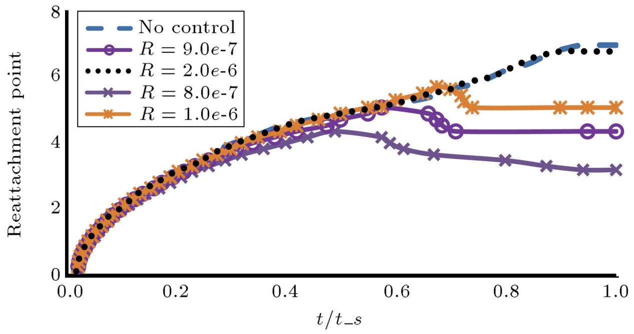

Figure 14. Variation of reattachment length with respect to time with and without controlling blowing/suction jets for Case C1 (t_s is a time of steady state flow).

constant R becomes smaller. The separation region is reduced by 54% for the case with $R = 8 \times 10^{-7}$. Time variation of the reattachment length in different controlling conditions, based on different values of the positive constant R (see Figure 12) and without a controller, is presented in Figure 14. It is obvious that the separation zone is suppressed at all times for unsteady flow over the step. Streamlines with and without control behind the step, at different times, are presented in Figure 15. They clearly indicate that the separation bubble is suppressed by the action of the controller. For further investigation of the accuracy of

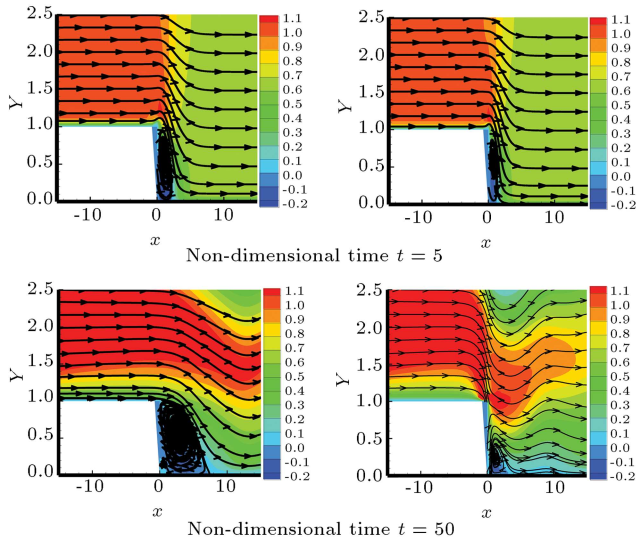

Figure 15. Streamlines and x-velocity contours at different times for Case C1 (left without control, right with blowing/suction jet control, $R = 8.0 \times 10^{-7}$).

the proposed model, the results of the controlling case using the perturbation method, for two different times (at $R = 8.e-7$), are compared with RANS solutions in Figure 16. We conclude that the accuracy of the perturbation method will be increased as the ε_p and non-dimensional time are reduced.

The next objective is to comment on the CPU time required for solving the perturbed RANS equations in comparison to the RANS equations with blowing/suction jet actuators. For the flow Reynolds number of 44000, the residual histories for solving the set of equations A and B with the impulse input as the controlling jet velocity in steady state form, are shown in Figure 17. From this figure, perturbed flow equations that are linear successfully accelerate convergence, compared to solving nonlinear RANS equations. Therefore, in performing optimal control theory, the consumption of CPU time for computing perturbed equations is much less than that for cases of solving RANS equations.

Case C2: The computational domain is similar to Case C1. The blowing/suction jets are located at the wall of the step (blowing at the foot and suction at $0.7H_s$). Optimal control input or perturbation parameter variation, with respect to non-dimensional time, and for different values of positive constant R, is shown in Figure 18. Controlling results indicate that the perturbation parameter increases with time and becomes constant when steady state condition is reached. The horizontal velocity contours, with and without control, at a non-dimensional time of 50, are shown in Figure 19. As indicated in velocity contours, the separation region has been effectively eliminated by the action of the controlling jets for the case of

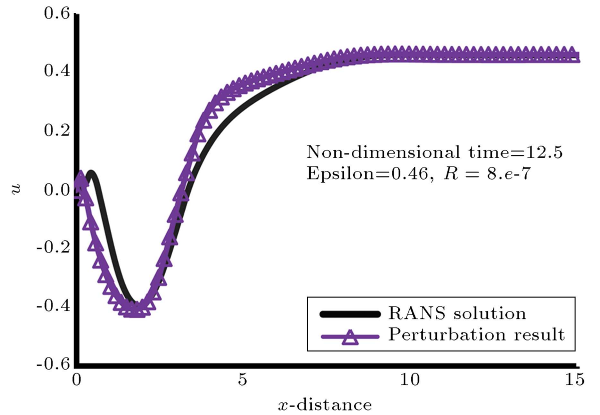

(a)

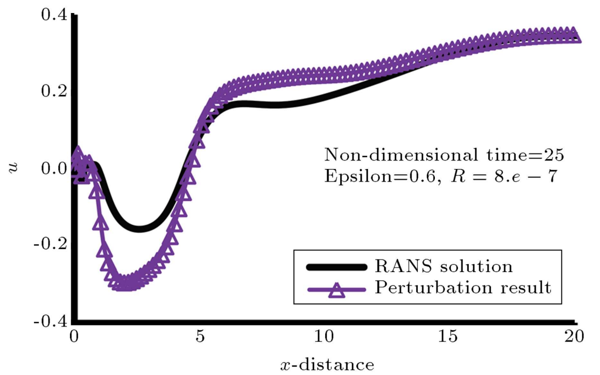

(b)

Figure 16. Comparison of the x-velocity profiles computed by different methods of the RANS solution and perturbation method with a pair of blowing/suction controlling jets for Case C1.

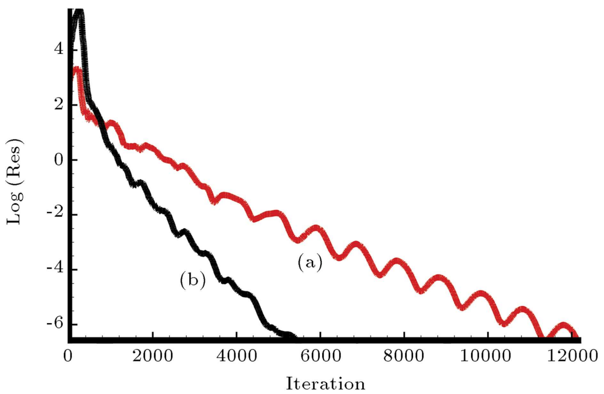

Figure 17. Residual histories for solving RANS equations: (a) Perturbed RANS equations, (b) with impulse input as control input in steady state form for Case C1.

$R = 1.e-9$. It is obvious that the location of the blowing/suction jets is crucial for the optimal performance of the controller. Unlike Case C1, the curvature of the streamlines is smooth and the controlling jets completely suppress the separated region.

From the CPU time analysis, it can be concluded that application of the perturbation method on the

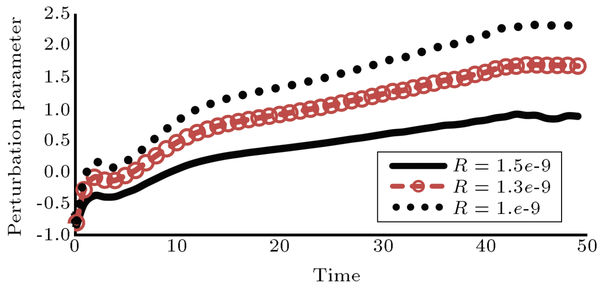

Figure 18. Control input variation with respect to time for Case C2 with a Reynolds number of 44000.

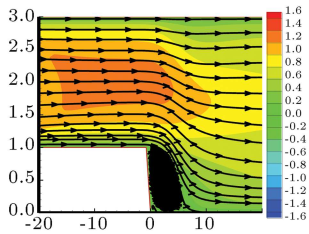

(a) No control

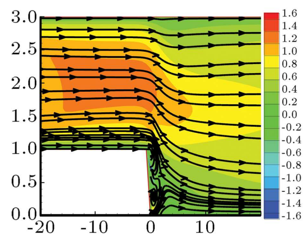

(b) R = 1.e-9

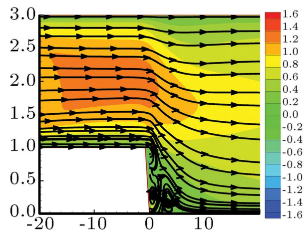

(c) R = 1.3e-9

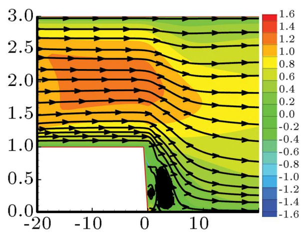

(d) R = 1.5e-9

Figure 19. x-velocity contours with and without control for Case C2.

RANS equations in solving the optimal control problem is beneficial. Besides, it can be shown that the perturbation method is more accurate in comparison to the classical POD method used by Ravindran [6]. To study the performance of the perturbation method, the simulation of flow control over backward-facing is carried out. The control is performed through blowing on the portion of the boundary near the step foot in the form:

$$(u, v) = \begin{cases} (c(t)30y(\frac{1}{4} - y), 0) & 0 \leq y \leq \frac{1}{4} \\ (0, 0) & \frac{1}{4} < y \leq 1 \end{cases}. \tag{36}$$

Values of control input or perturbation parameter, $c(t)$, for turbulent flow over a step with flow Reynolds number of 44000 can be estimated by the perturbation parameter, ε_p, presented in Figure 12. A specific case, with positive constant $R = 8.0 \times 10^{-7}$, is chosen for further investigation. To study the performance of the perturbation and POD methods, turbulent fluid flow over a step is simulated by three different methods:

Method 1. *RANS simulation:* The turbulent flow over the step with flow Reynolds number of 44000 is simulated by solving RANS equations with the RNG $k-\varepsilon$ turbulent model. A blowing jet near the step foot in the form of Eq. (36), with $c(t) = \varepsilon_p$, for a specific case of $R = 8.0 \times 10^{-7}$, is used as a controller.

Method 2. *Perturbation method:* RANS equations (set of equations A) are solved firstly without any control input. Then, perturbed flow equations (set of equations B) are solved with the controlling jet. In this case, impulse input or perturbation parameter, $c(t) = \varepsilon_p = 1$ (Eq. (36)), is used as the controller. Finally, the flow field with a specific control input of $c(t) = \varepsilon_p$ is computed by Eq. (21).

Method 3. *POD method:* From the POD method of Ravindran [6], the velocity expansion is defined as:

$$\mathbf{u}(\mathbf{x}, t) = \mathbf{u}^*(\mathbf{x}) + \sum_{j=1}^{n} a_j(t)\boldsymbol{\varphi}_j(\mathbf{x}) + c(t)\mathbf{u}_c(\mathbf{x}), \qquad (37)$$

where:

$$\mathbf{u}_c(\mathbf{x}) = \frac{\mathbf{u}_{c_1}(\mathbf{x}) - \mathbf{u}_{c_0}(\mathbf{x})}{c_1 - c_0}, \qquad (38)$$

and $\mathbf{u}_{c_1}(\mathbf{x})$ is a steady state flow velocity with a blowing controlling jet in the form of $c(t) = 1$, and $\mathbf{u}_{c_0}(\mathbf{x})$ is steady state flow velocity with $c(t) = 0$ for the blowing controlling jet. The snapshots are defined as $\mathbf{u}(\mathbf{x}, t_k) - c(t_k)\mathbf{u}_c(\mathbf{x})$. Overall, by inserting the velocity expansion (Eq. (37)) into RANS equations and using a Galerkin projection method, a set of ordinary differential equations for the time coefficients, $a_j(t)$, is obtained. By calculating these coefficients and using the controlled values of $c(t) = \varepsilon_p$, similar to the perturbation method (Figure 12), the flow field can be simulated by applying Eq. (37). The first and second POD modes used in these calculations are plotted in Figure 20. Results of the different simulation methods are presented in Figure 21. X-velocity profiles at different stations behind the step show that the perturbation method is more accurate than the POD method. This is mainly because the effect of a controller on the flow field is partially considered (through the perturbation method).

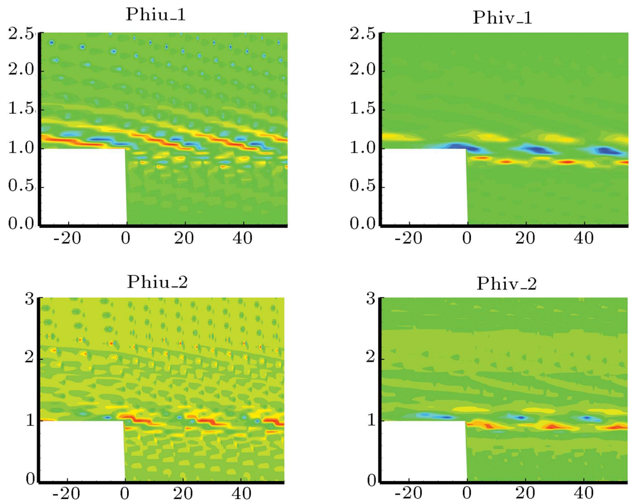

Figure 20. First and second POD modes.

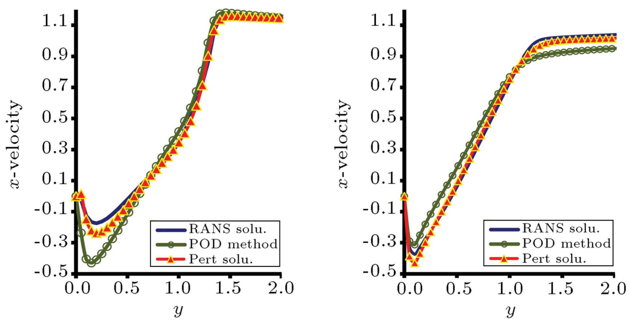

(a) Non-dimensional time=22.5

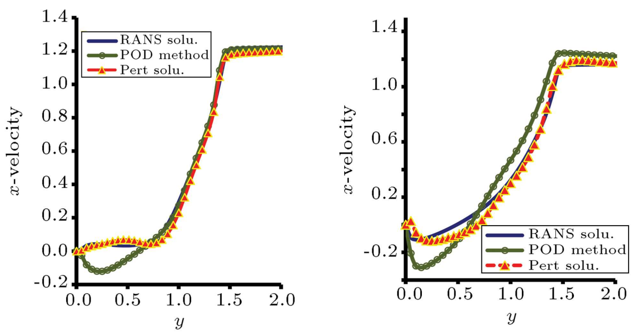

(b) Non-dimensional time=37.5

Figure 21. The controlled and uncontrolled flow velocity profiles at different stations (RANS solution, POD method and perturbation method).

6. Conclusion

The control of turbulent flow separation behind a backward-facing step using a POD low dimensional model and the perturbation method has been presented. The POD Galerkin projection reduces RANS equations to a low dimensional model. The disadvantages of this model are that the controlling parameter or inputs, such as blowing/suction jet velocity, do not show up explicitly in the resulting system and the flow field will not sense the effect of the controller in an optimal control process. The perturbation method introduced in this article on RANS equations is capable of handling these problems. In this way, the control parameter is inserted into the reduced order system explicitly, which is useful for control purposes, and the effect of the controller will be sensed by the flow field during the optimal control process. Therefore, the system can capture the time varying influence of the control input and predict RANS responses to an actuator accurately. This method is more accurate than the classical POD method used previously. Numerical results show that the perturbation method is more efficient and faster (can save about 50% of CPU time) in predicting controlling parameters for the turbulent flow over the step. In addition, it can be concluded that if the separation region is small, the perturbation method can predict the flow field more accurately. Two different controlling cases are investigated: Blowing/suction jets at the foot and the edge of the step and blowing/suction jets at the wall of the step. Results show that the position of the actuator is essential for the best performance of the controller. A blowing/suction jet at the wall of the step is more effective, and the separation region is removed completely as a result of the surface actuator.

References

1. Heenan, A.F. and Morrison, J.F. "Passive control of back step flow", *Experimental Thermal and Fluid Science*, **16**, pp. 122-132 (1998).
2. Jaňour, Z. and Jonáš, P. "On the flow in a channel with a backward-facing step on one wall", *Engineering Mechanics*, **1**, pp. 313-320 (1994).
3. Hanna, R. "Hypersonic shockwave/turbulent boundary-layer interactions on a porous surface", *AIAA Journal*, **33**, pp. 1977-9 (1995).
4. Boiko, A.V., Dovgal, A.V. and Hein, S. "Control of a laminar separation boundary layer induced stationary perturbations", *European Journal of Mechanics B/Fluids*, **27**, pp. 466-476 (2008).
5. Ravindran, S.S. "Control of flow separation over a forward-facing step by model reduction", *Computer Methods in Applied Mechanics and Engineering*, **191**, pp. 4599-4617 (2002).
6. Ravindran, S.S. "A reduced-order approach to optimal control of fluids using proper orthogonal decomposition", *International Journal for Numerical Methods in Fluids*, **34**, pp. 425-448 (2000).
7. Jaňour, Z. and Jonáš, P. "Some methods of the control of the separation region behind a backward facing step", *Proceeding in Applied Mathematics and Mechanics*, **4**, pp. 438-439 (2004).
8. Kiwan, S. "Using localized wall discharge to control the fluid flow and heat transfer for the flow over a backward facing step", *International Journal of Numerical Methods for Heat & Fluid Flow*, **18**, pp. 745-765 (2008).
9. Dejoan, A. and Leschziner, M.A. "Large eddy simulation of periodically perturbed separated flow over a backward-facing step", *International Journal of Heat and Fluid Flow*, **25**, pp. 581-592 (2004).
10. Dejoan, A., Jang, Y.J. and Leschziner, M.A. "Comparative LES and unsteady RANS computations for a periodically-perturbed separated flow over a backward-facing step", *Journal of Fluids Engineering*, **127**, pp. 872-878 (2005).
11. Šarić, S., Jakirlić, S. and Tropea, C. "A periodically perturbed backward-facing step flow by means of LES, DES and T-RANS: An example of flow separation control", *Journal of Fluids Engineering*, **127**, pp. 879-887 (2005).
12. Berkooz, G., Holmes, P. and Lumly, J.L. "The proper orthogonal decomposition in the analysis of turbulent flows", *Annual Review of Fluid Mechanics*, pp. 539-575 (1993).
13. Aubry, N., Holmes, P., Lumely, J.L. and Stone, E. "The dynamics of coherent structures in the wall region of a turbulent boundary layer", *Journal of Fluid Mechanics*, **192**, pp. 115-173 (1988).
14. Rowley, C.W., Colonius, T. and Murray, R.M. "Model reduction for compressible flows using POD and Galerkin projection", *Physica D*, **189**, pp. 115-129 (2004).
15. Zare, A., Emdad, H. and Goshtasbirad, E. "Feedback control of laminar flow behind backward-facing step by POD analysis and using perturbed Navier-Stokes equations", *Proceeding of the IMechE, Part C: Journal of Mechanical Engineering Science*, **226**, pp. 648-659 (2011).
16. Kasnakoğlu, C., Serrani, A. and Efe, M.O. "Control input separation by actuation mode expansion for flow control problems", *International Journal of Control*, **81**, pp. 1475-1492 (2008).
17. Ravindran, S.S. "Reduced-order controllers for control of flow past airfoil", *International Journal for Numerical Methods in Fluids*, **50**, pp. 531-554 (2006).
18. Yakhot, V., Orszag, S.A., Thangman, S., Gatski, T.B. and Speziale, C.G. "Development of turbulence models for shear flows by a double expansion technique", *Physics of Fluids*, **4**, pp. 1510-1520 (1992).
19. Jin, X., Cheng, D., Yang, W. and Jin, H. "Comparison of turbulence models on the prediction of flow field around a cube based on RANS", In: *Proceedings of Wind Engineering Conference (APCWE-VI)*, Seoul Korea, **6**, p. 54 (2005).
20. Wilcox, C.D., *Turbulence Modeling for CFD*, Birmingham Press, Inc. San Diego, California (2004).
21. Patankar, S.V., *Numerical Heat Transfer and Fluid Flow*, Hemisphere Washington DC (1980).
22. Sirovich, L. "Turbulence and dynamics of the coherent structures Part: I-III", *Quarterly of Applied Mathematics*, **45**, pp. 561-590 (1987).
23. Kirk, D., *Optimal Control Theory: An Introduction*, Englewood Cliffs, New Jersey: Prentice Hall (1970).
24. Kim, J., Kline, S.J. and Johnston, J.P. "Investigation of a reattaching turbulent shear layer: Flow over a backward-facing step", *Journal of Fluids Engineering*, **102**, pp. 302-308 (1980).

Appendix A

Quasi-linearization algorithm of Kirk [23]: Consider the 2n set of nonlinear differential control equations (Eq. (32)) as:

$$\dot{\mathbf{a}}(t) = f_1\left(\mathbf{a}(t), \boldsymbol{\lambda}(t), t\right),$$

$$\dot{\boldsymbol{\lambda}}(t) = f_2\left(\mathbf{a}(t), \boldsymbol{\lambda}(t), t\right),$$

$$\mathbf{a}(t_o) = \mathbf{a}_o \boldsymbol{\lambda}(t_f) = \boldsymbol{\lambda}_f. \tag{A.1}$$

As described by Kirk [23] for the first step, it is necessary to linearize these nonlinear differential equations by expanding them in Taylor series about a known trajectory $\mathbf{a}^i(t)$, $\boldsymbol{\lambda}^i(t)$ and retaining only first order terms in the expansion:

$$\begin{aligned}\dot{\mathbf{a}}^{i+1}(t) =& f_1\left(\mathbf{a}^i(t), \boldsymbol{\lambda}^i(t), t\right) + \frac{\partial f_1}{\partial a}\left(\mathbf{a}^i(t), \boldsymbol{\lambda}^i(t), t\right)\\ &\left[\mathbf{a}^{i+1}(t) - \mathbf{a}^i(t)\right] + \frac{\partial f_1}{\partial \boldsymbol{\lambda}}\left(\mathbf{a}^i(t), \boldsymbol{\lambda}^i(t), t\right)\\ &\left[\boldsymbol{\lambda}^{i+1}(t) - \boldsymbol{\lambda}^i(t)\right],\\ \dot{\boldsymbol{\lambda}}^{i+1}(t) =& f_2\left(\mathbf{a}^i(t), \boldsymbol{\lambda}^i(t), t\right) + \frac{\partial f_2}{\partial \mathbf{a}}\left(\mathbf{a}^i(t), \boldsymbol{\lambda}^i(t), t\right)\\ &\left[\mathbf{a}^{i+1}(t) - \mathbf{a}^i(t)\right] + \frac{\partial f_2}{\partial \boldsymbol{\lambda}}\left(\mathbf{a}^i(t), \boldsymbol{\lambda}^i(t), t\right)\\ &\left[\boldsymbol{\lambda}^{i+1}(t) - \boldsymbol{\lambda}^i(t)\right].\end{aligned} \tag{A.2}$$

The above equations can be re-ranged in the following form:

$$\dot{a}^{i+1}(t) = A_{11}\mathbf{a}^{i+1}(t) + A_{12}\boldsymbol{\lambda}^{i+1}(t) + A_{13},$$

$$\dot{\boldsymbol{\lambda}}^{i+1}(t) = A_{21}\mathbf{a}^{i+1}(t) + A_{22}\boldsymbol{\lambda}^{i+1}(t) + A_{23}, \tag{A.3}$$

where the coefficient matrices are:

$$A_{11} = \frac{\partial f_1}{\partial \mathbf{a}}, \quad A_{12} = \frac{\partial f_1}{\partial \boldsymbol{\lambda}},$$

$$A_{13} = -A_{11}\mathbf{a}(t) - A_{12}\boldsymbol{\lambda}(t) + f_1,$$

$$A_{21} = \frac{\partial f_2}{\partial \mathbf{a}}, \quad A_{22} = \frac{\partial f_2}{\partial \boldsymbol{\lambda}},$$

$$A_{23} = -A_{21}\mathbf{a}(t) - A_{22}\boldsymbol{\lambda}(t) + f_2. \tag{A.4}$$

The coefficient matrices are evaluated based on $\mathbf{a}^i(t)$ and $\boldsymbol{\lambda}^i(t)$ which are known. An initial guess should be defined to evaluate these matrices at the beginning of the first iteration. The next step is to solve homogeneous differential equations as:

$$\dot{\mathbf{a}}^{i+1}(t) = A_{11}\mathbf{a}^{i+1}(t) + A_{12}\boldsymbol{\lambda}^{i+1}(9t),$$

$$\dot{\boldsymbol{\lambda}}^{i+1}(t) = A_{21}\mathbf{a}^{i+1}(t) + A_{22}\boldsymbol{\lambda}^{i+1}(t). \tag{A.5}$$

By numerical integration, these set of equations should be solved with the following form of boundary conditions:

$$\mathbf{a}^{H1}(t_o) = \ldots = \mathbf{a}^{Hn}(t_o) = \mathbf{0},$$

$$\begin{aligned}\boldsymbol{\lambda}^{H1}(t_o) &= \begin{bmatrix}1 & 0 & 0 & \ldots & 0\end{bmatrix}^T \ldots \boldsymbol{\lambda}^{n1}(t_o)\\ &= \begin{bmatrix}0 & 0 & 0 & \ldots & 1\end{bmatrix}^T.\end{aligned} \tag{A.6}$$

Solutions of these homogeneous set of equations will be defined as $(\mathbf{a}^{H1}, \boldsymbol{\lambda}^{H1}), \cdots, (\mathbf{a}^{Hn}, \boldsymbol{\lambda}^{Hn})$. After that, it is recommended to generate one particular solution with boundary condition of $\mathbf{a}^p(t_o) = \mathbf{a}_o$, $\boldsymbol{\lambda}^p(t_o) = \mathbf{0}$. The solution at this stage is denoted by $\mathbf{a}^p$ and $\boldsymbol{\lambda}^p$. As we linearized original equations, the complete solution of Eq. (A.1) can be estimated using principle of superposition. The solution will be written as:

$$\mathbf{a}^{i+1}(t) = \omega_1\mathbf{a}^{H1}(t) + \ldots + \omega_n\mathbf{a}^{Hn}(t) + \mathbf{a}^p(t),$$

$$\boldsymbol{\lambda}^{i+1}(t) = \omega_1\boldsymbol{\lambda}^{H1}(t) + \ldots + \omega_n\boldsymbol{\lambda}^{Hn}(t) + \boldsymbol{\lambda}^p(t). \tag{A.7}$$

For the next stage the values of $\boldsymbol{\omega} = \begin{bmatrix}\omega_1 & \ldots & \omega_n\end{bmatrix}$ should be determined. As discussed by Kirk [23] we have:

$$\boldsymbol{\omega} = \left[\lambda^{H1}(t_f) \vdots \ldots \vdots \lambda^{Hn}(t_f)\right]^{-1} \left[\lambda_f - \lambda^p(t_f)\right]. \tag{A.8}$$

Then, by substituting values of $\boldsymbol{\omega}$ into Eq. (A.7), the new trajectory will be obtained. The solution of the original nonlinear equations can be obtained iteratively until converged solution is performed. In conclude the system of Eq. (A.1) must be solved using the following boundary conditions:

$$\mathbf{a}(t_o) = \mathbf{a}_o, \quad \boldsymbol{\lambda}(t_o) = \omega. \tag{A.9}$$

The iterative procedure for solving nonlinear two-point boundary-value problems can be summarized as:

1. Guess the initial trajectory for the state and costate variables $\mathbf{a}^i(t)$ and $\boldsymbol{\lambda}^i(t)$ where $t \in [t_0, t_f]$ and $i = 1$;
2. Evaluate the coefficient matrices of Eq. (A.4) on the trajectory $\mathbf{a}^i(t)$ and $\boldsymbol{\lambda}^i(t)$;
3. Numerically integrate set of homogenous differential Eq. (A.5) for $t \in [t_0, t_f]$ using n sets of initial conditions as Eq. (A.6). Particular solution is obtained by solving sets of Eq. (A.3) with boundary conditions of $\mathbf{a}^p(t_o) = \mathbf{a}_o$ and $\boldsymbol{\lambda}^p(t_o) = \mathbf{0}$;
4. Use the values found in step 3 to determine the vector ω from Eq. (A.8);
5. Use ω in step 4 and Eq. (A.7) to determine $(i+1)$st trajectory;

6. Compare the ith and $(i+1)$st trajectories by evaluating the norm error=$\left\| \begin{bmatrix} \mathbf{a}^{i+1} \\ \boldsymbol{\lambda}^{i+1} \end{bmatrix} - \begin{bmatrix} \mathbf{a}^{i} \\ \boldsymbol{\lambda}^{i} \end{bmatrix} \right\| < 10^{-5}$;
7. If error $< 1.e - 5$, the iterative procedure has converged; go to step 7, otherwise add 1 to i and go to step 2;
8. Integrate Eq. (A.1) with initial condition of $\mathbf{a}(t_o) = \mathbf{a}_o$ and $\boldsymbol{\lambda}(t_f) = \boldsymbol{\omega}$.

Biographies

Azam Zare received a BS degree from the Persian Gulf University, Iran, in 2000, and MS (local preconditioning for inviscid and viscous flow equations) and PhD (feedback control of separated flows by POD analysis, using perturbed Navier-Stokes equations) degrees from Shiraz University, Iran, in 2004 and 2011, respectively, all in Mechanical Engineering.

She has taught various courses at the Islamic Azad University, in Marvdasht, Iran, including statics, fluid mechanics, thermodynamics, engineering mathematics and internal combustion engines. Her computer skills include Intel® Fortran Visual Studio, Mathlab, Fluent and Gambit software, and she has written CFD programs in FORTRAN, with which she has studied the solution of Navier-Stokes equations for flow over different geometries. Her research interests include fluid mechanics, CFD and flow control. She has published a number of papers in various national and international journals in these areas.

Homayoon Emdad studied Mechanical Engineering. His research interests include: Fluid Mechanics, CFD, turbulent flow and flow control. He has taught various courses such as Fluid Mechanics, Computational Fluid Dynamic, Aerodynamic, Low Speed Aerodynamic, Engineering Mathematics for Bachelor Degree and Master Degree students in Shiraz University. His computer skills include Intel® Fortran, Visual Studio, Fluent and Gambit software. He wrote some CFD programs in FORTRAN and studied about solving Navier-Stokes equations for flow over different geometries in different flow regimes including laminar and turbulent.

Ebrahim Goshtasbi Rad studied Mechanical Engineering, including fluid mechanics, CFD, and turbulent flow and flow control. He has taught various courses in fluid mechanics, statics, turbo-machinery, pipeline systems, boundary layer, and gas dynamics for BS and MS degree students at Shiraz University, Iran. His computer skills include Intel® Fortran, Visual Studio, Epanet, Fluent and Gambit software.

He has published a number of papers in national and international journals in various areas of Mechanical Engineering,